RSC Advances

PAPER

View Article Online
View Journal | View Issue

Cite this: *RSC Adv.*, 2022, **12**, 22331

Synthesis, photophysical and nonlinear optical properties of push–pull tetrazoles†

Anna-Kay West, Lukas J. Kaylor, Mahamud Subir and Sundeep Rayat *

A 2,5-disubstituted tetrazole with *p*-nitrophenyl and 3-pyridyl units as acceptors (**1a**), and three push–pull tetrazoles with *p*-nitrophenyl as an acceptor and phenyl (**1b**), 2-(dibenzo[*b*,*d*]furan-4-yl) (**1c**), and 4-(*N*,*N*-diphenylamino)phenyl (**1d**) as donor groups, were synthesized by copper-catalyzed aerobic C–N coupling of *p*-nitrophenyl tetrazole with appropriately substituted aryl boronic acids. The absorption and emission spectra of **1a–c** showed minimal dependence on the polarity of the solvent; however, in the case of **1d** a blue shift was noted in the longest absorption band (λ_1) as the polarity increased. The fluorescence intensity of the title compounds was found to be solvent-dependent; however, no apparent correlation to solvent polarity could be established. The absorption and emission characteristics of **1a–d** were also influenced by the nature of the substituent as **1d**, bearing a strong electron donating 4-(*N*,*N*-diphenylamino)phenyl group, displayed a significant red shifted absorption (λ_1) as well as emission (λ_{em}) bands compared to other compounds. Time dependent density functional calculations (CAM-B3LYP/6-311++G**) revealed that the longest wavelength band (λ_1) is associated with an intramolecular charge transfer (ICT) from HOMO/HOMO-1/HOMO-2 → LUMO/LUMO+1 in these molecules. The first hyperpolarizability values, β_{HRS}, of **1a–d** were measured using the solution-based hyper-Rayleigh scattering technique using a femtosecond Ti:Sapphire laser and the highest NLO activity was measured for **1d** with the greatest push–pull characteristics. A strong correlation was observed between the calculated hyperpolarizability (β_{tot}) and experimentally measured values (β_{HRS}).

Received 13th July 2022
Accepted 27th July 2022

DOI: 10.1039/d2ra04307f

rsc.li/rsc-advances

Introduction

Organic push–pull molecules with a delocalized π-system exhibit highly efficient optoelectronic properties and show great promise as active components in the design of organic light-emitting diodes,[1] photodiodes,[2] solar cells[3] and nonlinear optical (NLO) devices.[4–6] Their unique spectroscopic properties are attributed to an intramolecular charge transfer (ICT) from the electron donating (D) to the electron accepting group (A) separated by a π-linker.[7] ICT generates a molecular dipole and polarization that imparts distinct electronic, linear and nonlinear optical properties to the molecule.[8] Materials with a strong NLO effect have applications in telecommunications, optical data storage, optical switching, and high performance computing.[9–12] The optical properties of push–pull molecules can be optimized by modifying the strength of D and A groups as well as the length and nature of the π-linker,[13,14] thereby amplifying the ICT and increasing the NLO response.[8]

The most commonly used electron donors are based on positive mesomeric or inductive effect (+M/+I) that include substituents such as –OH, –OR, $–NH_2$, or $–NR_2$ as well as heteroaromatic rings such as thiophenes.[8] Similarly, the widely employed electron acceptors exhibit negative mesomeric or inductive effect (–M/–I) that comprise of $–NO_2$, –CN, –CHO, –COOH groups as well as heterocycles such as pyridine, imidazoles, benzothiazoles, benzooxazoles and many others.[8] Push-pull chromophores containing the heterocyclic cores – oxazoles,[15–19] oxadiazoles[20–23] and triazoles[24,25] have received much attention in recent years, however, studies on the photophysical and NLO properties of the related tetrazole-based molecular systems are scarce in the literature. For instance, photophysical properties of compounds containing a tetrazole scaffold have been reported.[26–28] In addition, several coordination polymers involving tetrazole as a ligand have shown to display NLO properties[29–32] and a few substituted tetrazoles exhibit second harmonic generation (SHG),[33] however, to the best of our knowledge no NLO properties have been reported on tetrazole based push–pull systems. This may be because tetrazoles are typically regarded as conjugation disruptors due to the presence of a tertiary amine center that is expected to interrupt ICT from donor to the acceptor. Note that Diederich and coworkers have

Department of Chemistry, Ball State University, Foundational Sciences Building, Muncie, IN 47306, USA. E-mail: srayat@bsu.edu

† Electronic supplementary information (ESI) available: UV spectra of **1a–d** and the molar absorptivity values of different bands in various solvents; emission spectra of **1a–d** in different solvents; TDDFT simulated UV spectra of **1a–d** and vertical excitation energies, oscillator strengths and MO% contributions; hyper-Rayleigh scattering data; correlation of β_{tot} *vs.* β_{HRS}; Cartesian coordinates of **1a–d** optimized at CAM-B3LYP/6-311++G**; NMR spectra of the synthesized compounds. See https://doi.org/10.1039/d2ra04307f

reported modest to strong ICT in donor–acceptor substituted 1,2,3-Triazoles where the latter serves as a conjugative π-linker despite the presence of a tertiary amine center at N-1.[34] Other reports of charge transfer in donor–triazole–acceptor materials have also subsequently appeared in the literature.[35–37] Whether a tetrazole moiety could also serve as a conjugative π-linker between the donor and acceptor units leading to ICT remains unexplored to date. Since, NLO properties are directly dependent on efficient ICT, push–pull tetrazoles warrant investigation.

Herein, we employ a combination of experimental and computational methods to reveal how changes in the donor strength affect the photophysical properties of push–pull compounds based on tetrazoles. Four 2,5-disubstituted tetrazoles **1a–d** were synthesized *via* copper catalyzed C–N coupling of *p*-nitrophenyl tetrazole with aryl boronic acids in the presence of oxygen (Fig. 1). **1a** is not strictly a push–pull compound as both *p*-nitrophenyl and pyridyl units are electron acceptors and is included for comparison. In **1b–d**, the *p*-nitrophenyl moiety serves as an acceptor and electron donating groups consist of phenyl (**1b**), 2-(dibenzo[*b*,*d*]furan-4-yl)- (**1c**), and 4-(*N*,*N*-diphenylamino)phenyl (**1d**) groups. The absorption and emission properties of **1a–d** were investigated in different solvents and the density functional theory (CAM-B3LYP/6-311++G**) was utilized to rationalize the UV data as well as to predict the hyperpolarizability values. Note that the first order hyperpolarizabilities can be directly correlated to NLO properties of a material.[38] Experimentally, the hyperpolarizability values were investigated by employing solution-based hyper-Rayleigh scattering (HRS) technique using a femtosecond Ti:Sapphire laser. To our knowledge, this is the first study that reports NLO properties of 2,5-disubstituted push–pull tetrazoles.

Results and discussion

Synthesis

Recently, we reported that the synthesis of 2,5-diaryl tetrazolones can be efficiently carried out using Cu_2O nanoparticles as catalysts *via* the C–N coupling of aryl tetrazolones with aryl boronic acids.[39] With nanoparticles, the reaction was completed in shorter times and required relatively low catalyst loading compared to the amorphous catalyst. In this work, using Cu_2O nanoparticles, we successfully synthesized related 2,5-diaryltetrazoles **1a–d** by the reaction of 5-(4-nitrophenyl)-2*H*-tetrazole **3**[40] and aryl boronic acids in dry DMSO under an oxygen atmosphere (Scheme 1). The crude **1a–d** were purified by recrystallization and subjected to full spectral characterization.

Photophysical properties

Spectroscopic studies of **1a–d** were conducted in five solvents of increasing polarity that included toluene, 1,4-dioxane, chloroform, acetonitrile, and dimethyl sulfoxide. The complete UV-Vis absorption data in all solvents can be found in the ESI (Table S1 and Fig. S1–S5†). The molar absorptivity values were also obtained that suggest that all bands are $\pi \rightarrow \pi^*$ in nature. Our data reveals that changing the polarity of the solvent produced a meager effect on the absorption characteristics of **1a–c**. However, in case of **1d**, switching from solvents with low dielectric constant (*e.g.* toluene, dioxane and chloroform) to solvents of high dielectric constant (such as DMSO and acetonitrile), produced 8–14 nm blue shift in the longest absorption band (λ_1) (Table 1). This negative solvatochromism may be attributed to the better stabilization of the ground state compared to the excited state of **1d** by solvents of high polarity and is indicative of a decrease in dipole moment in the excited state.[41] The longest absorption band (λ_1) is most red shifted for **1d** compared to **1a–c** in all solvents (Fig. 2 and Table 1). This is attributed to the strong electron donating ability of the (*N*,*N*-diphenylamino)phenyl group which creates an efficient push–pull system.

The fluorescence spectra of **1a–d** were obtained in different solvents and all compounds were found to emit light, albeit weakly in some cases (see ESI, Fig. S6–S9†). We note that the emission band of **1d** is bathochromically shifted in all solvents compared to **1a–c**, owing to a greater degree of charge transfer from the donor to acceptor (Table 1). The spectra of **1a–d** in dioxane are shown in Fig. 3 (left).

We observed that the emission intensity was dependent on the solvent, as **1a** and **1b** showed a higher emission in dioxane compared to other solvents (Fig. S6 and S7†). In contrast, the emission maximum of **1a** and **1b** was not strongly affected by the solvent (Table 1). The fluorescence spectra of **1c** in all solvents displayed the vibrational fine structure typically observed in compounds with rigid structure and exhibited Stokes shifts ($\Delta\lambda$) between 25–37 nm. Analogous to **1a** and **1b**, the emission intensity of **1c** was solvent dependent, however, it didn't seem to correlate with solvent polarity (Fig. S8†). The emission maximum of **1c** was solvent independent. On the other hand, compound **1d** exhibited strong solvent dependent emission with respect to both wavelength shift and intensity (Fig. 3, right). In chloroform, acetonitrile and DMSO, **1d**

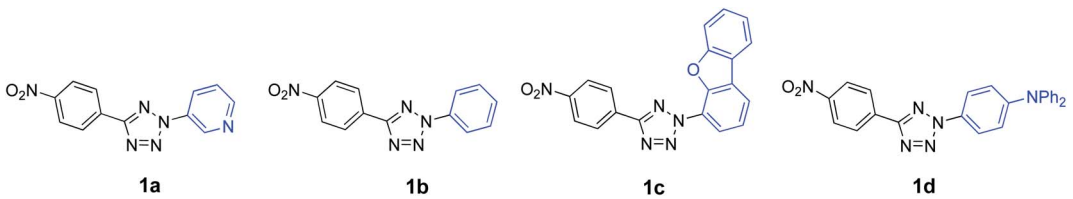

Fig. 1 2,5-Disubstituted tetrazoles **1a–d**.

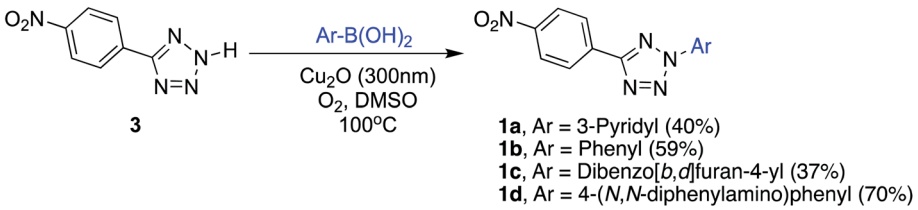

Scheme 1 C–N coupling of 5-(4-nitrophenyl)-2*H*-tetrazole **3** with boronic acids to obtain 2,5-diaryl tetrazoles **1a–d**.

Table 1 Photophysical properties of **1a–d**

	Toluene	Dioxane	$CHCl_3$	MeCN	DMSO
1a					
λ_1 (nm)	Insoluble	296	295	293	296
ε (M^{-1} cm^{-1})		27 000	25 000	24 000	20 000
λ_{em}[a] (nm)		350, 550	Weak	Weak	Weak
$\Delta\lambda$ (nm)		46			
1b					
λ_1 (nm)	300	295	298	295	300
ε (M^{-1} cm^{-1})	21 000	25 000	24 000	23 000	21 000
λ_{em}[a] (nm)	338	340, 572	Weak	Weak	Weak
$\Delta\lambda$ (nm)	38	55			
1c					
λ_1 (nm)	290	288	289	287	288
ε (M^{-1} cm^{-1})	28 000	33 000	26 000	30 000	29 000
λ_{em}[a] (nm)	316	316	317	315	316
$\Delta\lambda$ (nm)	26	28	37	25	29
1d					
λ_1 (nm)	374	368	370	360	360
ε (M^{-1} cm^{-1})	20 000	23 000	18 000	30 000	18 000
λ_{em}[a] (nm)	540	569	460	493, 532	489, 535
$\Delta\lambda$ (nm)	166	202	90	133	129

[a] Excitation was at λ_1.

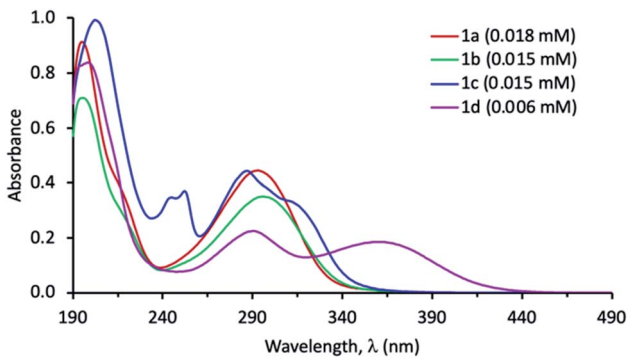

Fig. 2 UV-Vis absorption spectra of **1a–d** in acetonitrile.

displayed relatively weak fluorescence. However, when non-polar solvents, such as toluene and dioxane were used, the emission band was red shifted with a remarkable enhancement in fluorescence intensity, which is greatest in toluene. Typically, push–pull systems are known to display (i) red shift with increasing solvent polarity which is attributed to the stabilization of a polar emitting excited state involving ICT as well as (ii) fluorescence quenching in polar solvents due to the lowered energies of the ICT states.[42,43] In stark contrast, we note a blue shift in polar solvents while observing a decrease in emission intensity for **1d**. This suggests that the latter exhibits complex photophysical properties which warrants further investigation beyond the scope of this study. Another notable feature of **1d**, is its remarkably large Stokes shifts ($\Delta\lambda$) with values up to 200 nm in non-polar dioxane and 133 nm in polar aprotic solvent *e.g.* DMSO (Table 1). Such dyes with large Stokes shift in polar solvents such as DMSO are scarce and are highly sought for applications in bioimaging and biosensing.[44]

DFT calculations

Ground state geometries. To gain insights into the electronic properties, **1a–d** were optimized at CAM-B3LYP/6-311++G** and the structures are shown in Fig. 4. Molecules **1a** and **1b** display C_s symmetry while **1c** exhibit a dihedral angle of −40.5° between *p*-nitrophenyl tetrazolyl unit and dibenzofuranyl substituent which may be attributed to the repulsions between the lone pairs present on the N1 of the tetrazole and oxygen atom of the dibenzofuranyl ring. **1d** also exhibits a slight twist between the *p*-nitrophenyl tetrazolyl and the 4-(*N*,*N*-diphenylamino)phenyl units displaying a dihedral angle of 18°. The ground state dipole moment of **1a–d** is large (5.3, 6.9, 8.1, and 8.6 D, respectively) which suggests unsymmetrical charge distribution in the ground state which increases in the order **1a** → **1b** → **1c** → **1d**.

Frontier molecular orbitals. The isodensity plots of the frontier molecular orbitals **1a–d** at CAM-B3LYP/6-311++G** are depicted in Fig. 5. All molecular orbitals (MO) display π-type symmetry, except HOMO-2 of **1a** which is a σ MO localized on the pyridyl unit. HOMO-2 of **1b–d** is delocalized over the entire molecule. In case of **1a**, HOMO-1 is confined to the *p*-nitrophenyl group. In **1b**, it is mainly localized on the phenyl ring and in **1c**, HOMO-1 is concentrated on the dibenzofuranyl ring with some contribution from the tetrazole. In case of **1d**, HOMO-1 is delocalized over the entire molecule. HOMO of **1a** and **1b** is delocalized over the entire molecule, while in case of **1c** and **1d**, this MO is exclusively localized on the donor substituents, *i.e.* the dibenzofuranyl and 4-(*N*,*N*-diphenylamino) phenyl units. LUMO of **1a–d** is entirely concentrated on the acceptor, the *p*-nitrophenyl group with small contribution from the tetrazole ring. This MO feature is characteristic of the push–pull molecular systems and suggests that transitions from HOMO or HOMO-1 → LUMO can contribute to ICT in these molecules. The LUMO+1 for **1a–d** is restricted to the tetrazole

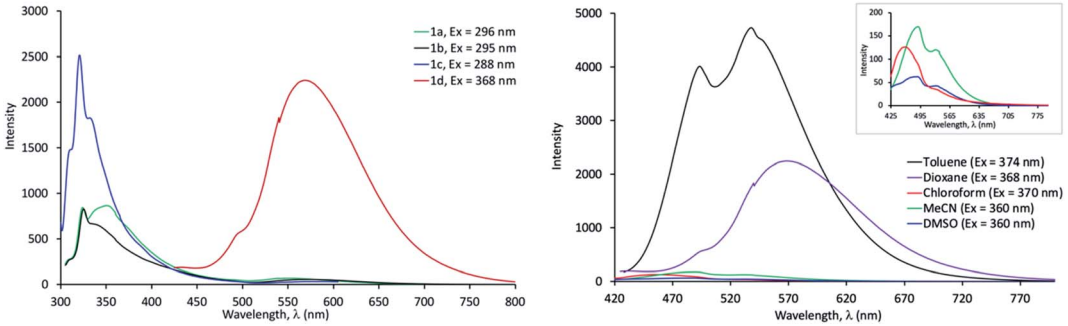

Fig. 3 Emission spectra of **1a–d** in dioxane (right) and of **1d** (left) in various solvents (inset shows spectra in chloroform, acetonitrile and DMSO). The absorbance of the solutions ranging between 0.1–0.15 (in a 1 cm path length) were used to collect emission at the excitation wavelength. (Sharp signals observed in case **1a** and **1b** may be due to Raman scattering. The emission of **1c** was reproducible at different excitation wavelengths).

ring as well as the respective acceptor (pyridyl)/donor (phenyl, benzofuranyl, and anilino) fragments. The HOMO and LUMO energies in eV are given in Table 2. A small variation in LUMO energies of **1a–d** is noted ($E_{LUMO} = -1.73$ to -1.93 eV) which is consistent with the presence of the identical acceptor (*p*-nitrophenyl group), while the HOMO energies ranged between $E_{HOMO} = -6.87$ to -8.81 eV, which are reflective of the electronic effects imposed by presence of different acceptor/donors in **1a–d**. Furthermore, the HOMO → LUMO band gap narrows in the order **1a** > **1b** > **1c** > **1d** which is suggestive of the increased push–pull character.

Vertical excitation energies. To determine the nature of the electronic transitions that give rise to bands in the UV spectra of **1a–d**, time-dependent density functional calculations (TDDFT CAM-B3LYP/6-311++G**) were carried out in acetonitrile and thirty low lying singlet excited states of **1a–d** were calculated (Fig. S10–S13†). The calculated UV spectra were found to be in good agreement with the experimental spectra (Fig. S1–S5†). The vertical excitation energies, their oscillator strength, main MO% contributions and transition type for the most intense transitions in acetonitrile are shown in Table S2.† The analysis of TDDFT wavefunction of **1a** and **1b** reveals that the longest absorption band λ_1 that is experimentally observed at 293 and 295 nm in acetonitrile, respectively, mainly corresponds to a transition from HOMO → LUMO and is theoretically calculated to be at 285 and 288 nm (Table S2†). In case of **1c**, λ_1 is experimentally found as well as theoretically predicted at 287 nm, and consists of mixture of transitions mostly from HOMO-2 → LUMO and HOMO-1 → LUMO. For **1d**, λ_1 is observed at 360 nm and is calculated at 340 nm by TDDFT and

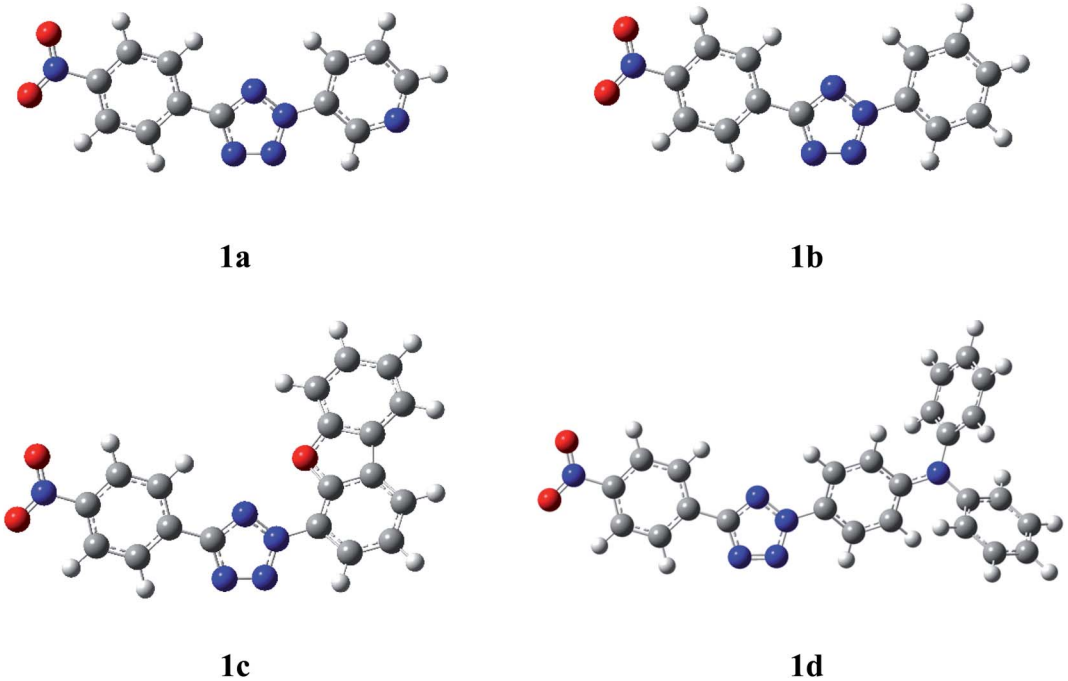

Fig. 4 CAM-B3LYP/6-311++G** optimized geometries of tetrazoles **1a–d**.

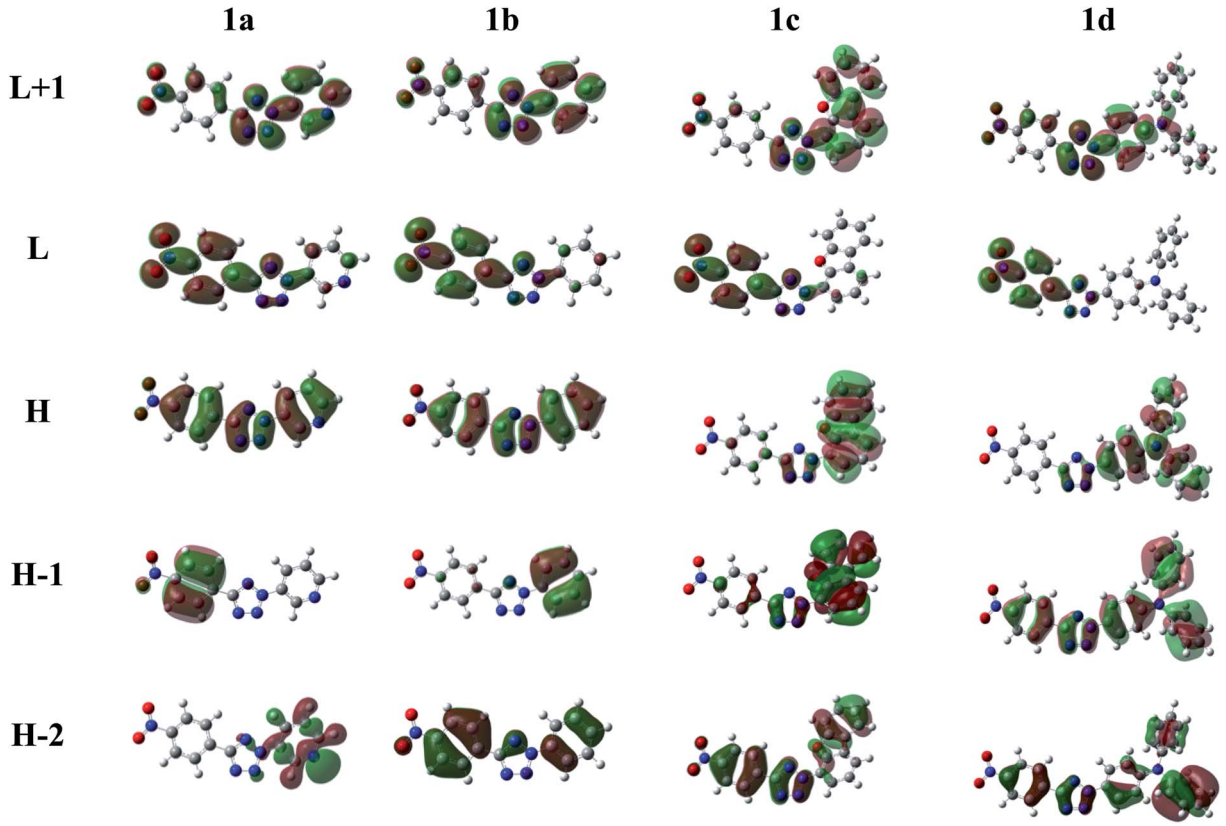

Fig. 5 Isodensity plots of the molecular orbitals of **1a–d** at CAM-B3LYP/6-311++G**.

comprises of transitions from HOMO → LUMO and HOMO → LUMO+1. The main MO% contributions for other bands of **1a–d** (λ_2 and λ_3) can also be found in Table S2.† These are composed of several excited states consisting of transitions between different molecular orbitals of comparable energy.

Intramolecular Charge Transfer (ICT). The analyses of MOs confirm that the lowest energy band (λ_1) band in **1a–d** is of $\pi \rightarrow \pi^*$ in nature, in agreement with the experimentally measured molar absorptivity values (Table 1), and is associated with an ICT which becomes prominent as the push–pull character increases. While **1a** is not strictly a push–pull system as both *p*-nitrophenyl and pyridyl rings are electron acceptors, however, examination of the MOs reveal similarities with that of **1b** where λ_1 excitation corresponds to a weak ICT due to presence of a weak donor (phenyl, $\sigma = -0.01$). Note that HOMO in **1a** and **1b** is delocalized over the entire molecule, while LUMO is concentrated on the acceptor, the *p*-nitrophenyl unit (Fig. 5), suggesting a weak CT in both. The visualization of the MOs involved in the formation of λ_1 of **1c** indicate a moderate degree of ICT as HOMO-2 is spread over the entire molecule, HOMO-1 is localized on the donor group while LUMO is concentrated on the acceptor. However, in **1d**, the isodensity plots of MOs associated with transitions leading to λ_1 indicate that HOMO is mostly restricted on the 4-(*N*,*N*-diphenylamino)phenyl group, while the LUMO and LUMO+1 are exclusively localized on the *p*-nitrophenyl unit or the tetrazolyl-anilino unit, respectively, suggestive of a more pronounced ICT from donor to acceptor. Analogous to experimental observations, TDDFT predicts bathochromic shift in the position of λ_1 with the introduction of a strong electron donating group in **1d**. Thus, our computational work supports the hypothesis that a tetrazole moiety could also serve as a conjugative π-linker (analogous to triazoles[34,36]) between the donor and acceptor fragments leading to ICT.

Nonlinear optical (NLO) properties

The polarization created by the ICT in **1a–d** prompted us to evaluate the NLO response from these molecules under induction by light irradiation. Since, the first order hyperpolarizabilities can be directly correlated to NLO properties of a material,[38] these values (β_{tot}) were calculated using CAM-B3LYP/6-311++G** as described in the computational methods.[45] We first calculated the β_{tot} value for *p*-nitroaniline in $CHCl_3$ which was found to be 32.3×10^{-30} esu, in good

Table 2 HOMO and LUMO energies, and band gaps (in eV) at CAM-B3LYP/6-311++G**

	HOMO	LUMO	$\Delta E_{L\rightarrow H}$
1a	−8.81	−1.93	6.88
1b	−8.56	−1.81	6.75
1c	−8.22	−1.73	6.49
1d	−6.87	−1.90	4.97

agreement with the experimental value ($23(\pm3) \times 10^{-30}$ esu in chloroform[46]). This suggested that CAM-B3LYP/6-311++G** is a reliable method to calculate hyperpolarizability values of organic molecules, also validated by others.[47–49] The calculated β_{tot} values were found to be in the order **1d** ≫ **1b** > **1a–1c** (Table 3). Compound **1d** is predicted to exhibit highest β_{tot} value due to small HOMO–LUMO band gap that results into more efficient charge transfer. Note that chromophores carrying the 4-(*N*,*N*-diphenylamino)phenyl group have also been previously reported to display large nonlinearities.[43] Our calculations also show that β_{tot} in the studied molecules is dominated by β_{xxx}. When compared to urea ($\beta_{tot} = 0.066 \times 10^{-30}$ esu at CAM-B3LYP/6-31+G**[50]) which is a standard NLO material, the predicted values for **1a–d** are 383, 474, 381, 1652 times higher.

Experimentally, the hyperpolarizability, β_{HRS}, values of **1a–d** were determined in chloroform by the hyper-Rayleigh scattering (HRS) method. Based on this technique, the total corrected HRS intensity from the solution at the second harmonic frequency, 2ω, can be expressed as:[46,51]

$$I_{2\omega} = g\,(N_{solvent}\beta^2_{solvent} + N_{solute}\beta^2_{solute})I^2_{\omega} = gB^2I^2_{\omega}.$$

This equation shows a quadratic dependence of the $I_{2\omega}$ on the intensity (or power) of the incident beam at the fundamental frequency, ω. The factor g depends on the detection geometry, which is fixed, and thus remains a constant throughout the experiment. Assuming dilute solution, a plot of $I_{2\omega}$ as a function of incident power allows determination of the quadratic coefficients, gB^2, for solutions of different solute concentrations. From the slope of the gB^2 *vs.* N_{solute} plot and the known literature value of β_{CHCl_3} (-4.9×10^{-31} esu),[46] the β_{HRS} for the target compound is obtained.

Table 3 Hyperpolarizability tensors and first order hyperpolarizability (β_{tot}) calculated at CAM-B3LYP/6-311++G** as well as experimental values (β_{HRS}) in chloroform ($\times10^{-30}$ esu)

	1a	1b	1c	1d
β_{xxx}	26.79	−32.32	−21.63	106.64
β_{xxy}	5.6	5.26	10.68	−3.67
β_{xyy}	−1.5	0.45	−3.4	−4.41
β_{yyy}	−0.72	−1.28	−3.55	4.19
β_{xxz}	−0.0005	−0.001	2.06	−1.21
β_{xyz}	−0.0002	0.0001	−0.42	−2.13
β_{yyz}	−0.0001	0.0001	0.75	0.24
β_{xzz}	−0.44	0.82	0.98	−0.67
β_{yzz}	0.24	0.18	−0.35	−0.09
β_{zzz}	0.0002	0.00003	0.24	−0.04
β_{tot}	25.4	31.3	25.2	101.6
β_{HRS}	30 ± 13	47 ± 2	30 ± 16	252 ± 23

Fig. 6 shows a representative dataset for the **1b**. As discussed above, by fitting the plot of $I_{2\omega}$ against incident power (Fig. 6, left), the quadratic coefficient, gB^2, is obtained at different solute (**1b**) concentrations and subsequently, these values are then plotted as a function of N_{solute} (or number density), which has been obtained by multiplying concentration of **1b** with Avogadro's number (Fig. 6, right). The concentrations of the solutions are reported within the plots. Using the fitting parameters, β_{HRS} has been determined. The standard deviation has been calculated based on propagation of error from the uncertainties in the slope and the *y*-intercept of the gB^2 *vs.* N_{solute} plot.

The β_{HRS} values of **1a–d** in chloroform at the excitation wavelength of 800 nm are reported in Table 3. The associated plots for all the molecules are shown in the ESI, Fig. S14.† It is observed that the compound **1d** displays a strong NLO activity ($\beta_{HRS} = 252(\pm16) \times 10^{-30}$ esu). As a comparison, using a similar technique, the β_{HRS} of *p*-nitroaniline has been reported to be $23(\pm3) \times 10^{-30}$ esu in chloroform[46] at the excitation wavelength of 1064 nm. It can be seen in the UV-Vis spectra (Fig. 2), **1d** exhibits an electronic transition near 400 nm. Thus, we attribute this relatively large β_{HRS} to a resonance enhancement at 400 nm. It must be noted, **1d** also displayed a strong two photon fluorescence. The relative β_{HRS} trend for the compounds is: **1d** ≫ **1b** > **1a–1c** . This appears to be consistent with the relative magnitude of the transition dipole moment, μ_{eg}, of these compounds (Table S2†) as the first molecular hyperpolarizability is proportional to μ_{eg} and the difference in the permanent dipole moment of the ground and excited states.[52] While further investigations with respect to wavelength dependence and solvent effect on β_{HRS} are warranted, these data not only indicate the effect of donor–acceptor pair investigated herein but also highlight that by tuning the substituents

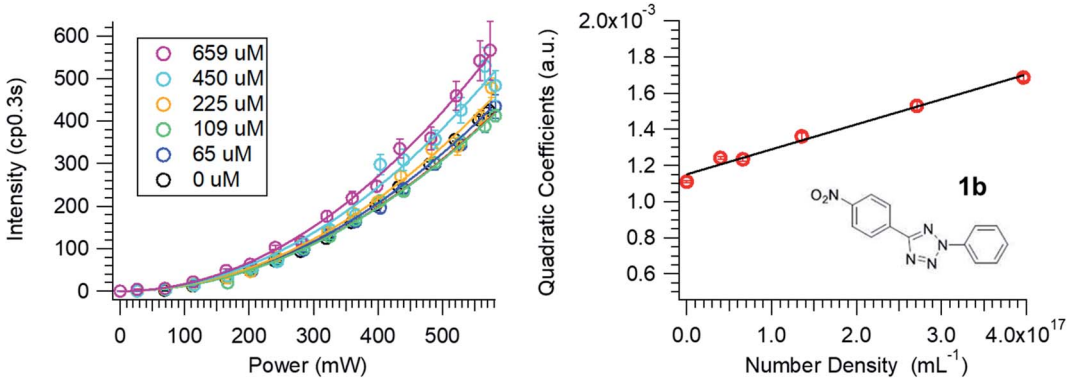

Fig. 6 $I_{2\omega}$ *vs.* incident power (left) and the quadratic coefficients gB^2 *vs.* N_{solute} plots for **1b**. N_{solute} is referred as number density in the plot.

of tetrazole-based compounds, achieving large first molecular hyperpolarizability is plausible.

Overall, a good correlation between predicted values β_{tot} and experimentally determined β_{HRS} was observed (Table 3 and Fig. S15†), however, the β_{tot} for **1d** was greatly underestimated. Note that different molecular conformations can lead to significantly different hyperpolarizabilities due to differences in the instantaneous dipole moment or interruption of the π-conjugation pathway. Since it is impossible to predict the exact conformation that a molecule adopts in solution, discrepancies are often observed between theoretically and experimentally calculated hyperpolarizability values. This factor is more pronounced in **1d** due to its inherent high degree of freedom owing to the presence of 4-(*N*,*N*-diphenylamino)phenyl group, compared to **1a–c** which are more rigid.

Conclusions

Synthesis of **1a–d** *via* aerobic C–N coupling of *p*-nitrophenyl tetrazole **3** with the corresponding boronic acids in the presence of Cu_2O nanoparticles as catalyst proceeded smoothly. Our studies showed that the photophysical properties of **1a–d** can be tuned with substituents, especially by adding a strong electron donor such as 4-(*N*,*N*-diphenylamino)phenyl group. The solvent effects on the photophysical properties of **1a–d** were small, except for **1d** where a blue shift in the absorption and emission bands is observed with increasing solvent polarity. The emission intensity of all compounds was found to be solvent dependent, although no correlation to solvent polarity can be discerned. In general, non-polar solvents showed enhanced fluorescence intensity and greater red shift of the emission maximum for **1d** compared to the polar solvents, resulting in large Stokes shifts. Ground state dipole moment of **1a–d** indicate unsymmetrical charge distribution suggestive of a CT character. TDDFT analyses further show that excitation from HOMO/HOMO-1/HOMO-2 → LUMO/LUMO+1 make dominant contributions to the lowest energy band (λ_1) of **1a–d** and corresponds to ICT. In compound **1a** this may be attributed to the difference in the electron accepting ability of two groups, $-NO_2$ being a stronger acceptor than 3-pyridyl group with Hammett substituents constants (σ) of 0.79 (ref. 53) and 0.45,[53] respectively. A significant increase in ICT is noted for **1d** carrying the strong electron donor, the 4-(*N*,*N*-diphenylamino)phenyl group. Furthermore, the theoretically calculated (β_{tot}) and experimentally measured (β_{HRS}) values of **1a–d** exhibit a good correlation and demonstrate that tuning the substituents and the donor–acceptor strengths allow for achieving moderate to strong NLO activity in this class of tetrazole compounds. Application of these compounds in frequency doubling processes is thus plausible; however, further studies are needed to elucidate a relationship between their molecular structure and SHG efficiency.

Finally, our work shows that analogous to triazoles,[34,36] the related tetrazole can act as a conjugative π-linker, and tetrazoles substituted with donor and acceptor groups display weak to strong ICT. Although **1d** has weak emission in DMSO, its large Stokes shift makes it an interesting candidate for further optimization of photophysical properties for potential applications in bioimaging and biosensors. Overall, compounds **1a–d** exhibit interesting photophysical properties that warrant further investigation which will be reported in due course.

Experimental

All boronic acids were commercially obtained and purified by recrystallization, as necessary. DMSO for C–N coupling reactions was dried by stirring over molecular sieves (4 Å) for 3 days (fresh molecular sieves were used every 24 h). DMSO was collected by centrifugation. Thin layer chromatography was conducted on silica plates and visualized under UV light. The ^{1}H and ^{13}C NMR spectra were recorded on a JEOL 400 MHz spectrometers in DMSO-d_6 or $CDCl_3$ as indicated. The NMR spectra were processed using Mnova software. Chemical Shift is expressed in parts per million (ppm) relative to the solvent signal. In the ^{1}H NMR spectral data, the multiplicity (s = singlet, d = doublet, t = triplet, m = multiplet), coupling constant *J* (in Hz) and integration (number of protons) are expressed in parenthesis. Low resolution mass spectra were obtained on a mass spectrometer equipped with an electrospray ion source operated in the positive ion mode and connected to a linear ion trap mass analyzer. UV spectra were obtained on Shimadzu UV 2600 spectrophotometer and emission spectra were obtained on JASCO FP-8350 Spectrofluorometer. For fluorescence measurements, the bandpass was set at 5 nm for both excitation and emission. DMSO and acetonitrile used for UV and emission measurements were spectroscopic grade, chloroform used was HPLC grade and both dioxane and toluene were reagent grade (>99%). For NLO, HPLC grade chloroform was used.

Synthesis of 5-(4-nitrophenyl)-2*H*-tetrazole 3[40]

Sodium azide (781 mg, 12 mmol), urea (721 mg, 12 mmol) and water (5 mL) were added to a round bottom flask and stirred at 60 °C for 1 h. In a separate flask, 4-nitrobenzonitrile (1 g, 6.8 mmol), acetic acid (1 mL) and dimethylformamide (DMF) (5 mL) were mixed and heated to 60 °C in an oil bath. After 1 h, the mixture containing 4-nitrobenzonitrile was added to the sodium azide solution at 60 °C. The reaction mixture was heated to 110 °C and stirred under reflux for 8-10 h. After completion of reaction as indicated by TLC, the mixture was cooled to room temperature and diluted with distilled water (5 mL) and ethyl acetate (10 mL) followed by the addition of 5 N aqueous hydrochloric acid (5 mL). The resulting mixture was stirred at room temperature for 30 min. The organic layer was separated and washed with 40% aqueous sodium chloride solution (5 mL) thrice and dried over anhydrous sodium sulphate. The solvent was removed under reduced pressure. The crude product was a yellow solid and was dried under high vacuum. (778 mg, 60%), R_f (hexane : dichloromethane 5 : 5) 0.11; ^{1}H NMR (400 MHz, DMSO-d_6): δ = 7.94 (s, 1H), 8.30 (d, J = 8.4 Hz, 2H), 8.45 (d, J = 8.4 Hz, 2H) ppm.

Synthesis of disubstituted tetrazoles 1a–d

General procedure. 5-(4-nitrophenyl)-2*H*-tetrazole **3** (0.76 mmol) was added to a round bottom flask containing aryl boronic acid (1.6 mmol) and Cu_2O nanoparticles (0.05 mmol) dissolved in dry DMSO (8 mL). The resulting mixture was placed in an oil bath at 100 °C for 8–10 hours under O_2. Upon completion of the reaction as indicated by TLC, the mixture was cooled to room temperature, diluted with ethyl acetate, consecutively washed with 1 M hydrochloric acid (HCl) and brine. The organic layer was collected, dried over anhydrous sodium sulphate and filtered. Solvent was removed under reduced pressure and the crude was purified by recrystallization from ethanol and characterized by NMR spectroscopy.

3-(5-(4-Nitrophenyl)-2*H*-tetrazol-2-yl) pyridine 1a. Compound **1a** was prepared from **3** (292 mg, 1.5 mmol) and phenylboronic acid (544 mg, 4.4 mmol) following the general procedure. Crude was purified by recrystallization that yielded a pale pink solid (159 mg, 40%); R_f (hexane : ethyl acetate 5 : 5) 0.63; ^{1}H NMR (400 MHz, Chloroform-*d*): $\delta = 7.58–7.61$ (m, 1H), 8.42 (d, $J = 8.9$ Hz, 2H), 8.48 (d, $J = 8.9$ Hz, 2H), 8.53 (d, $J = 8.2$ Hz, 1H), 8.82 (d, $J = 4.6$ Hz, 1H), 9.52 (s, 1H) ppm. ^{13}C NMR (100 MHz, Chloroform-*d*): 124.36, 124.48, 127.3, 128.1, 132.6, 133.4, 141.4, 149.3, 151.3, 164.0. Anal. calcd for $C_{12}H_8N_6O_2$: C, 53.73; H, 3.01; N, 31.33. Found: C, 54.00; H, 2.97; N, 31.22.

5-(4-Nitrophenyl)-2-phenyl-2*H*-tetrazole 1b. Compound **1b** was prepared from **3** (500 mg, 2.6 mmol) and phenylboronic acid (634 mg, 5.2 mmol) following the general procedure. Crude was recrystallized yielding off-white solid (410 mg, 59%), R_f (hexane : dichloromethane 7 : 3) 0.45; ^{1}H NMR (400 MHz, Chloroform-*d*): $\delta = 7.53–7.63$ (m, 3H), 8.22 (d, $J = 8.3$ Hz, 2H), 8.40 (d, $J = 9.1$ Hz, 2H), 8.46 (d, $J = 9.2$ Hz, 2H) ppm. ^{13}C NMR (100 MHz, Chloroform-*d*): 120.1, 124.4, 127.9, 129.9, 130.3, 133.2, 136.8, 149.2, 163.5. Anal. calcd for $C_{13}H_9N_5O_2$: C, 58.43; H, 3.39; N, 26.21. Found: C, 58.65; H, 3.43; N, 26.24.

2-(Dibenzo[*b*,*d*]furan-4-yl)-5-(4-nitrophenyl)-2*H*-tetrazole 1c. Compound **1c** was prepared from **3** (600 mg, 3.1 mmol) and dibenzofuran-4-boronic acid (1332 mg, 6.2 mmol) using the general procedure. Purification by recrystallization gave a pale pink solid (412 mg, 37%), R_f (hexane : ethyl acetate 5 : 5) 0.90; ^{1}H NMR (400 MHz, Chloroform-*d*): $\delta = 7.42$ (t, $J = 6.0$ Hz, 1H), 7.51 (t, $J = 6.3$ Hz, 2H), 7.64 (d, $J = 6.6$ Hz, 1H), 7.90 (d, $J = 6.1$ Hz, 1H), 7.96–7.99 (m, 2H), 8.20 (d, $J = 7.1$ Hz, 2H), 8.28 ppm (d, $J = 7.1$ Hz, 2H) ppm. ^{13}C NMR (100 MHz, Chloroform-*d*): 105.5, 111.9, 112.3, 113.0, 113.6, 114.0, 114.2, 114.6, 115.0, 117.7, 118.0, 118.4, 122.0, 133.0, 134.8, 140.9, 146.2. Anal. calcd for $C_{19}H_{11}N_5O_3$: C, 63.87; H, 3.10; N, 19.60. Found: C, 64.15; H, 3.26; N, 19.33.

4-(5-(4-Nitrophenyl)-2*H*-tetrazol-2-yl)-*N*,*N*-diphenyl aniline 1d. Compound **1d** was prepared from **3** (600 mg, 3.1 mmol) and 4-(*N*,*N*-diphenylamino) phenylboronic acid (1792 mg, 6.2 mmol) following the general procedure. Crude was recrystallized yielding yellow solid (949 mg, 70%), R_f (hexane : ethyl acetate 9 : 1) 0.85; ^{1}H NMR (400 MHz, Chloroform-*d*): $\delta = 7.14–7.21$ (m, 8H), 7.30–7.33 (m, 4H), 7.85 (d, $J = 7.2$ Hz, 2H), 8.16 (d, $J = 7.1$ Hz, 2H), 8.20 (d, $J = 7.1$ Hz, 2H) ppm. ^{13}C NMR (100 MHz, Chloroform-*d*): 112.3, 113.3, 114.9, 115.8, 117.8, 119.26, 119.56, 122.1, 132.9, 134.7, 135.3, 145.9. LRMS(ESI): m/z 435 ($M + H^+$). Anal. calcd for $C_{25}H_{18}N_6O_2$: C, 69.11; H, 4.18; N, 19.34. Found: C, 69.32; H, 4.18; N, 19.30.

Synthesis of copper(I) nanoparticles

In a 100 mL round bottom flask, 453 mg of copper acetate was dissolved in 25 mL of distilled water to produce a 0.1 M copper acetate solution. 25 mL of a 0.1 M sodium hydroxide solution was then added to the copper acetate dropwise. The solution was placed in an oil bath and stirred. Once the solution was at a temperature of 60 °C, it was removed from the oil bath and 25 mL of 0.1 M hydrazine was added dropwise. After the addition of hydrazine, the solution was placed back into the oil bath and stirred for 10 minutes. After 10 minutes, the solution was left to sit in the oil bath with no stirring for an extra 5–10 minutes. The solution was cooled, and the copper(I) nanoparticles were filtered through vacuum filtration. The nanoparticles were washed with distilled water (thrice) and 95% ethanol (once) then left to dry overnight at room temperature.

Absorption and emission spectroscopy

Stock solutions of **1a–d** were prepared in respective solvents which were diluted to prepare working solutions in the range 0.0018–0.0462 mM. UV spectra of these samples were recorded and are shown in Fig. S1–S5† with their respective concentrations. These were then used to determine molar absorptivities using Beer–Lambert law (Table S1†). For emission measurements, dilute solutions that showed absorption of 0.1 at the excitation wavelength were employed. The concentrations of these ranged between 0.0009–0.0030 mM and the path length was 1 cm.

Nonlinear optical (NLO) properties

NLO properties of the compounds **1a–d** were explored experimentally using the solution phase femtosecond hyper-Rayleigh scattering method.[46,51,52] In particular, the first molecular hyperpolarizabilities, β_{HRS}, of these compounds were measured in chloroform. A broadband Ti:Sapphire Tsunami oscillator (80 MHz with ~70 fs pulse width) (Spectra-Physics, 3941-X1BB), pumped by Nd:YVO_4 solid state laser (Spectra-Physics, Millennia eV), was used as the excitation light source at 800 nm. The general experimental setup has been described elsewhere,[54] with modifications made to accommodate HRS detection at a 90° angle from the incident beam. In brief, the incident beam was passed through various optics and then focused using a lens (focal length of 5.0 cm) at the center of a glass cuvette (3.5 mL, 1 cm pathlength) containing the solution under investigation. The sample was stirred and kept at a constant temperature (22 °C) using a temperature-controlled cuvette holder (Flash 300, Quantum Northwest). The power of the incident beam was modulated using a combination of two linear polarizers and a half waveplate. A long wavelength pass filter was used before the sample to remove unwanted second harmonic light and a short pass filter after the sample to block the fundamental beam. The generated light was collimated and focused into a monochromator (Acton SP2500, Princeton

Instruments). The signal was detected using a PMT (H11461, Hamamatsu), then amplified (SR445A) and processed using a gated photon counter (SR400) (Stanford Research Systems). The data was recorded and processed using a home-built LabVIEW program (National Instruments).

HRS measurements were performed within 24 hours of the solution preparation. For each solution and at a given incident beam power, HRS intensity, $I_{2\omega}$, has been measured as a function of wavelength in the range of 370 nm to 440 nm. A total of five spectra were collected and averaged. Each spectrum was fit to obtain the intensity peak at 400 nm. Fitting with double Gaussian function allowed eliminating the two-photon contribution, if any, to the overall signal. Similar method of subtracting background fluorescence has been established to be effective in a previous study.[55] The HRS intensity was then corrected based on Beer–Lambert law for possible attenuation of light due to molecular absorption. The concentrations of the solutions prepared are reported within the figures displaying the variation of harmonic intensity with concentration.

Computational methods

All calculations were carried out with Gaussian 09 package of programs[56] and employed Coulomb attenuating method CAM-B3LYP[57] in conjunction with 6-311++G** basis set. The CAM-B3LYP functional is widely utilized to calculate the absorption spectra of organic molecules as well as to predict the hyperpolarizability values of push–pull π-conjugated systems with reliability.[47–49] All the geometry optimizations were followed by vibrational analyses to ensure the positive sign of all eigenvalues of the Hessian matrix and to confirm that the stationary point found was a true minimum on the potential energy surface. Vertical excitation energies were computed in acetonitrile using time dependent density functional theory (TDDFT)[58] using the integral equation formalism of the polarized continuum model (IEFPCM) on the optimized ground state geometries in gas phase. The molecular orbitals were visualized using GaussView. The first hyperpolarizability values (β_{tot}) were calculated using the "polar" keyword in the Gaussian input file and by beginning the route section by #P that prints the static hyperpolarizability tensors. In order to consider the effect of solvent on the hyperpolarizability (β_{tot}), single point calculations were carried out in chloroform on the optimized ground state geometries using the IEFPCM model. β_{tot} was calculated as follows:[45]

$$\beta_{tot} = [(\beta_{xxx} + \beta_{xyy} + \beta_{xzz})^2 + (\beta_{yyy} + \beta_{xxy} + \beta_{yzz})^2 + (\beta_{zzz} + \beta_{xxz} + \beta_{yyz})^2]^{1/2}$$

where, β_{xxx}, β_{xyy}, β_{xzz}, β_{yyy}, β_{xxy}, β_{yzz}, β_{zzz}, β_{xxz} and β_{yyz} represent the hyperpolarizability tensor components along the x, y and z directions.

Author contributions

Anna-Kay West performed the synthesis and spectral characterization, completed UV measurements, prepared the pertaining figures and table, wrote the experimental section on the synthesis, performed preliminary data analysis. Lukas Kaylor collected the hyper-Rayleigh scattering (HRS) data and performed the analysis of hyperpolarizability. Mahamud Subir conceived and designed the analysis of hyperpolarizability measurement, collected the HRS data, performed the analysis of hyperpolarizability, wrote the section on the topic of HRS measurements and the corresponding results and conclusions. Sundeep Rayat conceived the project idea, designed the synthesis, collected the emission spectra, analyzed the UV and emission data, performed the computational work and subsequent data analysis as well as wrote the manuscript (except the HRS section).

Conflicts of interest

There are no conflicts to declare.

Acknowledgements

Low resolution mass spectrometric analyses were carried out on a LTQ XL mass spectrometer (ThermoFisher Scientific) supported by NSF-MRI grant under CHE-1531851. Computational work was performed on the Beowulf cluster supported by NSF-MRI grant CNS-1726017 and Ball State University. M. Subir would like to acknowledge Dr Yi Rao for useful discussions related to the NLO measurements and data analyses.

References

1 A. Haldi, A. Kimyonok, B. Domercq, L. E. Hayden, S. C. Jones, S. R. Marder, M. Weck and B. Kippelen, *Adv. Funct. Mater.*, 2008, **18**, 3056–3062.
2 H. Opoku, C. Bathula, E.-S. Shin, D. X. Long, H. Kong, Y. J. Jung, B. Lim and Y.-Y. Noh, *Org. Electron.*, 2020, **78**, 105580.
3 A. Labrunie, A. H. Habibi, S. Dabos-Seignon, P. Blanchard and C. Cabanetos, *Dyes Pigm.*, 2019, **170**, 107632.
4 C. Dengiz, *Turk. J. Chem.*, 2021, **45**, 1375–1390.
5 L. Mencaroni, C. Bonaccorso, V. Botti, B. Carlotti, G. Consiglio, F. Elisei, C. G. Fortuna, A. Spalletti and A. Cesaretti, *Dyes Pigm.*, 2021, **194**, 109620.
6 D. A. Zainuri, M. Abdullah, M. F. Zaini, H. Bakhtiar, S. Arshad and I. Abdul Razak, *PLoS One*, 2021, **16**, e0257808.
7 M. Klikar, P. Solanke, J. Tydlitat and F. Bures, *Chem. Rec.*, 2016, **16**, 1886–1905.
8 F. Bureš, *RSC Adv.*, 2014, **4**, 58826–58851.
9 A. Nayak, J. Park, K. De Mey, X. Hu, T. V. Duncan, D. N. Beratan, K. Clays and M. J. Therien, *ACS Cent. Sci.*, 2016, **2**, 954–966.
10 F. Ortiz-Trejo, M. Trejo-Valdez, J. P. Campos-Lopez, J. H. Castro-Chacon and C. Torres-Torres, *Appl. Sci.*, 2020, **10**, 5688.
11 R. Sharma, M. Singh and H. Kaur, *J. Mater. Sci.*, 2021, **56**, 2838–2855.

12 K. Mondal, S. Biswas, A. Pramanik, D. Banerjee, V. Rao Soma, A. Kumar Chaudhary and P. Kumbhakar, *Appl. Surf. Sci.*, 2022, **578**, 151966.
13 J. Kulhánek, F. Bureš, O. Pytela, T. Mikysek, J. Ludvík and A. Růžička, *Dyes Pigm.*, 2010, **85**, 57–65.
14 Y. Gong, X. Guo, S. Wang, H. Su, A. Xia, Q. He and F. Bai, *J. Phys. Chem. A*, 2007, **111**, 5806–5812.
15 Z.-H. Xing, J.-Y. Zhuang, X.-P. Xu, S.-J. Ji, W. Su and Z. Cui, *Tetrahedron*, 2017, **73**, 2036–2042.
16 F. Mahuteau-Betzer and S. Piguel, *Tetrahedron Lett.*, 2013, **54**, 3188–3193.
17 C. Sravani, M. Y. Lone, P. C. Jha, K. I. Sathiyanarayanan and A. Sivaramakrishna, *Spectrochim. Acta, Part A*, 2019, **210**, 171–180.
18 J. Sun, M. Zheng, J. Jia, W. Wang, Y. Cui and J. Gao, *Dyes Pigm.*, 2019, 164.
19 X. Liu, J. M. Cole, P. G. Waddell, T.-C. Lin, J. Radia and A. Zeidler, *J. Phys. Chem. A*, 2012, **116**, 727–737.
20 S. Chidirala, H. Ulla, A. Valaboju, M. R. Kiran, M. E. Mohanty, M. N. Satyanarayan, G. Umesh, K. Bhanuprakash and V. J. Rao, *J. Org. Chem.*, 2016, **81**, 603–614.
21 M. S. Najare, M. K. Patil, A. A. Nadaf, S. Mantur, S. R. Inamdar and I. A. M. Khazi, *Opt. Mater.*, 2019, **88**, 256–265.
22 A. Kurowska, P. Zassowski, A. S. Kostyuchenko, T. Y. Zheleznova, K. V. Andryukhova, A. S. Fisyuk, A. Pron and W. Domagala, *Phys. Chem. Chem. Phys.*, 2017, **19**, 30261–30276.
23 I. Mikhailov, Y. Artyushkina, G. Dushenko, O. Mikhailova, Y. Revinskii and V. Minkin, *Russ. J. Gen. Chem.*, 2018, **88**, 338–341.
24 M. M. Efremova, A. I. Govdi, V. V. Frolova, A. M. Rumyantsev and I. A. Balova, *Molecules*, 2021, **26**, 2801–2814.
25 C. Denneval, O. Moldovan, C. Baudequin, S. Achelle, P. Baldeck, N. Plé, M. Darabantu and Y. Ramondenc, *Eur. J. Org. Chem.*, 2013, **2013**, 5591–5602.
26 E. d. O. Zaldguer, R. d. C. Duarte, R. Cercená, F. d. S. Santos, L. G. T. A. Duarte, T. D. Z. Atvars, E. Zapp, D. Brondani, F. S. Rodembusch and A. G. Dal-Bó, *Dyes Pigm.*, 2022, **205**, 110574.
27 B. S. Arslan, Y. Derin, B. A. Misir, S. Kaya, I. Sisman, A. Tutar and M. Nebioglu, *J. Mol. Struct.*, 2022, **1267**, 133608.
28 K. Karrouchi, I. Celik, S. Fettach, T. Karthick, K. Bougrin, S. Radi, M. E. A. Faouzi, M. h. Ansar and R. Renjith, *J. Mol. Struct.*, 2022, **1265**, 133363.
29 R. T. Dong, Z. Y. Ma, L. X. Chen, L. F. Huang, Q. H. Li, M. Y. Hu, M. Y. Shen, C. W. Li and H. Deng, *CrystEngComm*, 2015, **17**, 5814–5831.
30 J.-Z. Liao, D.-C. Chen, F. Li, Y. Chen, N.-F. Zhuang, M.-J. Lin and C.-C. Huang, *CrystEngComm*, 2013, **15**, 8180–8185.
31 Y.-H. Tan, J.-X. Gao, Z.-F. Gu, Q. Xu, C.-S. Yang, Y.-S. Luo, B. Wang, Y.-Z. Tang and H.-R. Wen, *Polyhedron*, 2015, **101**, 239–243.
32 H. Zhou, K. Yang, Y. Liu, Y. Tang, W. Wei, Q. Shu, J. Zhao and Y. Tan, *Chin. Chem. Lett.*, 2020, **31**, 841–845.
33 M. Sahara, H. Ichioka, S. Yano, F. Fujimoto, M. Ehara, K. Wakita and N. Sonoda, *Jpn. J. Appl. Phys.*, 1994, **33**, 169–170.
34 P. D. Jarowski, Y.-L. Wu, W. B. Schweizer and F. Diederich, *Org. Lett.*, 2008, **10**, 3347–3350.
35 Y. Zhu, S. Guang, X. Su, H. Xu and D. Xu, *Dyes Pigm.*, 2013, **97**, 175–183.
36 P. Kautny, D. Bader, B. Stöger, G. A. Reider, J. Fröhlich and D. Lumpi, *Chem.–Eur. J.*, 2016, **22**, 18887–18898.
37 A.-S. Cornec, C. Baudequin, C. Fiol-Petit, N. Plé, G. Dupas and Y. Ramondenc, *Eur. J. Org. Chem.*, 2013, **2013**, 1908–1915.
38 J. S. Al-Otaibi, A. H. Almuqrin, Y. S. Mary and Y. S. Mary, *J. Mol. Struct.*, 2020, 1217.
39 T. E. Reason, B. Goka, J. A. Krause, A. K. Fionah, E. M. Zahran and S. Rayat, *CrystEngComm*, 2021, **23**, 3220–3229.
40 T. Jin, F. Kitahara, S. Kamijo and Y. Yamamoto, *Chem.–Asian J.*, 2008, **3**, 1575–1580.
41 S. Nigam and S. Rutan, *Appl. Spectrosc.*, 2001, **55**, 362A–370A.
42 H. Detert and V. Schmitt, *J. Phys. Org. Chem.*, 2004, **17**, 1051–1056.
43 E. V. Verbitskiy, S. Achelle, F. Bures, P. le Poul, A. Barsella, Y. A. Kvashnin, G. L. Rusinov, F. R.-l. Guen, O. N. Chupakhin and V. N. Charushin, *J. Photochem. Photobiol., A*, 2021, **404**, 112900.
44 T. He, Y. Wang, X. Tian, Y. Gao, X. Zhao, A. C. Grimsdale, X. Lin and H. Sun, *Appl. Phys. Lett.*, 2016, **108**.
45 A. Eşme and S. Sagdinc, *BAÜ Fen Bil. Enst. Dergisi*, 2014, **16**, 47–75.
46 K. Clays and A. Persoons, *Phys. Rev. Lett.*, 1991, **66**, 2980–2983.
47 C. Tonnele, B. Champagne, L. Muccioli and F. Castet, *Phys. Chem. Chem. Phys.*, 2018, **20**, 27658–27667.
48 J. Wei, P. Song, F. Ma, R. M. Saputra and Y. Li, *Opt. Mater.*, 2020, **99**, 109580.
49 Y. Liu, Y. Yuan, X. Tian, J. Yuan and J. Sun, *Int. J. Quantum Chem.*, 2020, **120**, e26176.
50 F. Mammadova, S. Ozsinan, M. Okutan and C. Dengiz, *J. Mol. Struct.*, 2020, **1220**, 128726.
51 K. Clays and A. Persoons, *Rev. Sci. Instrum.*, 1992, **63**, 3285–3289.
52 M. A. Pauley, C. H. Wang and A. K. Y. Jen, *J. Chem. Phys.*, 1995, **102**, 6400–6405.
53 D. H. McDaniel and H. C. Brown, *J. Org. Chem.*, 1958, **23**, 420–427.
54 C. B. Nelson, K. E. Shane, A. A. Al-Nossiff and M. Subir, *J. Phys. Chem. C*, 2015, **119**, 2630–2636.
55 Y. Rao, X.-m. Guo, Y.-S. Tao and H.-f. Wang, *J. Phys. Chem. A*, 2004, **108**, 7977–7982.
56 M. J. T. Frisch, G. W., H. B. Schlegel, G. E. Scuseria, M. A. C. J. R. Robb, V. G. Zakrzewski, J. A. Montgomery, R. E. B. Jr, J. C. Stratmann, S. Dapprich, J. M. Millam, A. D. K., K. N. Daniels, M. C. Strain, O. Farkas, J. Tomasi, V. C., M. Barone, R. Cammi, B. Mennucci, C. Pomelli, S. O. C. Adamo, J. Clifford, G. A. Petersson, P. Y. Ayala, Q. Cui, K. M., D. K. Morokuma, A. D. Rabuck, K. Raghavachari, J. B. C., J. Foresman, J. V. Ortiz,

A. G. Baboul, G. L. B. B. Stefanov, A. Liu, P. Piskorz, I. Komaromi, R. Gomperts, R. L. F., D. J. Martin, T. Keith, M. A. Al-Laham, C. Y. Peng, A. C., M. Nanayakkara, P. M. W. Gill, B. Johnson, M. W. A. W. Chen, J. L. Wong, C. Gonzalez, M. Head-Gordon, E. S. P. and J. A. Replogle, Gaussian Inc., Pittsburg, PA, 2003.

57 T. Yanai, D. P. Tew and N. C. Handy, *Chem. Phys. Lett.*, 2004, **393**, 51–57.

58 M. E. Casida, *Recent Adv. Comput. Chem.*, 1995, **1**, 155–192.